Advances in Colloid and Interface Science 167 (2011) 24–37

Contents lists available at ScienceDirect

Advances in Colloid and Interface Science

journal homepage: www.elsevier.com/locate/cis

Complexation and coacervation of polyelectrolytes with oppositely charged colloids

Ebru Kizilay [a,*], A. Basak Kayitmazer [b,*], Paul L. Dubin [a]

[a] Department of Chemistry, University of Massachusetts Amherst, MA 01003, United States
[b] Department of Chemistry, Bogazici University, Bebek, 34342 Istanbul, Turkey

ARTICLE INFO

Available online 8 July 2011

Keywords:
Complex coacervation
Polyelectrolyte-colloid interactions
Coacervate
Structure

ABSTRACT

Polyelectrolyte-colloid coacervation could be viewed as a sub-category of complex coacervation, but is unique in (1) retaining the structure and properties of the colloid, and (2) reducing the heterogeneity and configurational complexity of polyelectrolyte–polyelectrolyte (PE–PE) systems. Interest in protein-polyelectrolyte coacervates arises from preservation of biofunctionality; in addition, the geometric and charge isotropy of micelles allows for better comparison with theory, taking into account the central role of colloid charge density. In the context of these two systems, we describe critical conditions for complex formation and for coacervation with regard to colloid and polyelectrolyte charge densities, ionic strength, PE molecular weight (MW), and stoichiometry; and effects of temperature and shear, which are unique to the PE-micelle systems. The coacervation process is discussed in terms of theoretical treatments and models, as supported by experimental findings. We point out how soluble aggregates, subject to various equilibria and disproportionation effects, can self-assemble leading to heterogeneity in macroscopically homogeneous coacervates, on multiple length scales.

Published by Elsevier B.V.

1. Introduction

Complex coacervation is the separation of a macromolecular solution composed of two oppositely charged macroions into two immiscible liquid phases. In order to distinguish it from the simple coacervation of a single polymer, Bungenberg de Jong and Kruyt coined the name “complex coacervation” [1]. The dense liquid phase, which is relatively concentrated in macromolecules, is called the coacervate. While the definition of “coacervation” is clear, that of “coacervate” is not since it sometimes refers to the metastable suspension of macroion-rich droplets. Here “coacervate suspension” refers to the biphasic system, while the clear dense phase is defined as “coacervate”. This coacervate phase is more viscous and more concentrated than the initial solution, and exhibits a number of unique properties.

Complex coacervation was first investigated by Bungenberg de Jong for the system of gum arabic-gelatin [1]. His work was cited by Oparin who mentioned the similarity to proto-cells and coacervates, and Oparin proposed that life first formed in coacervate droplets. [3] The first theoretical model of complex coacervation was put forward by Voorn et al. [4] and following theoretical models were developed by Veis et al. [5], Nakajima and Sato[6], and Tainaka [7]. Coacervation can also take place for polyelectrolytes and oppositely charged colloids, e.g. micelles, [8,9] proteins [10] or dendrimers [11] (see Figs. 1 and 2). While it might be suggested that binding to polyelectrolytes induces micelle deformation or even disintegration, evidence for the full retention of micelle structure comes from (a) the absence of change in the solubilizing capacity of micelles regardless of whether they are free, complexed, or in coacervate [12] (b) the size of micelles within coacervates [13] and, indirectly, the strong influence of (free) micelle size and shape on the conditions for complexation and coacervation [14–16]. Colloid-PE coacervation, essentially its own field, has enormous potential due to the diverse functional properties of the proteins, micelles, and related colloids that replace the second PE. In this paper, it should be noted that “colloid” refers only to micelles and proteins, whose properties support a wide number of applications in foods, cosmetics, and pharmaceuticals. Polyelectrolyte-micelle systems are relevant to personal care products [17], are models for other colloidal systems since micelles have uniform shape and charge distribution). Polyelectrolyte-protein coacervates are particularly important in (i) enzyme immobilization [18], (ii) antigen delivery [19], (iii) design and production of biomaterials for cell micropatterning [20], (iv) protein purification [21], and (v) stabilization of food products [22]. More recently, a truly biological example of coacervates has been found: the mineralized tube of the sandcastle worm— formed from mineral particles glued together with cement made from coacervates of oppositely charged polypeptides (Fig. 3) [23].

The relationship between PE–PE coacervation and PE–colloid coacervation can be described in terms of similarities and differences. The identification of soluble complexes as precursors of coacervates seems to be better established for PE–protein [24] and PE–micelle [25] systems, with relatively few papers for PE–PE (e.g. gelatin A-gelatin B) systems [26]. For both types of complexes, it appears likely that large aggregates of the “primary” (intrapolymer) complexes are antecedents

* Corresponding authors.
E-mail addresses: ekizilay@chem.umass.edu (E. Kizilay), basak.kayitmazer@boun.edu.tr (A.B. Kayitmazer).

0001-8686/$ – see front matter. Published by Elsevier B.V.
doi:10.1016/j.cis.2011.06.006

Fig. 1. Typical coacervate suspensions (before centrifugation) of poly(dimethlydiallylammonium chloride) (PDADMAC)/sodium dodecyl sulfate (SDS)-Triton X-100, at Y = 0.4, I = 0.4 M NaCl (see Section 2.1).

of coacervates [8,27]. The approach toward coacervation for both systems usually involves charge neutralization, e.g. via alteration of the charge of one or both partner macroions, or alteration of the combining ratio (microstoichiometry) within the complex. It is difficult to know to what extent the concomitant aggregation is a consequence of neutralization or a true precondition for coacervation [28]. Either way, it is clear that for both categories of macroions, coacervate yield is maximal in the region of (bulk) 1:1 charge stoichiometry ("[+]/[−]") [29,30]. Charge complementarity is however another aspect of stoichiometry: when the oppositely charged macroions have highly dissimilar charge spacing, soluble complexes may be favored over coacervates even for [+]/[−] = 1. Moreover, the main entropy term for PE–PE coacervation and PE–colloid coacervation is counterion release.

Complex coacervation in colloid–PE differs from that in PE–PE systems in three important ways. First, colloidal macroions are less subject to MW and chemical polydispersity than most PE's studied, with consequences: First: (a) The heterogeneity of the PE–PE systems broaden all observed transitions including coacervation, so fundamental behavior as a true liquid–liquid phase transition is often masked; (b) The gain in PE configurational entropy that accompanies the transition to the presumably entangled coacervate – a network in which polymer chains are intermingled – from the more constrained complex should be less significant for the PE–colloid mixtures [31,32]. (c) Complexes of PE's with charged colloids can be linked both to models that describe the "condensation" of PE chains on colloidal surfaces [33,34] and to binding isotherm descriptions in the case of small colloids treated as ligands binding to "host" PE's. Such representations facilitate the interpretation of e.g. isothermal titration calorimetry (ITC) of PE-protein systems [35], whereas ITC for PE–PE systems is difficult to model [36,37]. (d) Compared to PE-reassembly, the structure and function of colloids may be fully retained during coacervation, e.g. with the preservation of enzyme activity [38] and micelle solubilization [39] leading to important applications.

In what follows, coacervation induced by colloid charge and the existence of soluble complexes as precursors of coacervation will be discussed in detail. Moreover, we will evaluate the effect of different key parameters such as ionic strength, polyelectrolyte charge density and PE molecular weight. Next, we discuss the thermodynamics leading to the formation of PE/colloid complexes and coacervates. We then present the mechanism, conditions and models of coacervation. The last section examines coacervate structures at different length scales.

2. Onset of complexation

2.1. pH_c and Y_c

Complex coacervation in colloid-polyelectrolyte systems occurs subsequent to the binding of polyions on colloid particles. Theoretical treatments of the adsorption of polyions on oppositely charged colloidal particles [34,40] have established that the onset of binding depends on the charge per polymer repeat unit (q), the ionic strength and the colloid charge density. Thus, at a given ionic strength, no interactions occur unless the colloid surface charge density exceeds a critical value, σ_c. All theoretical treatments lead to relationships such as Eq (1) [41]:

$$\sigma_c q \sim \kappa^b. \tag{1}$$

Here σ_c is the critical colloid surface charge density, q is the charge of a polymer repeat unit, and κ is the Debye–Huckel parameter. While Eq (1) is based on planar geometry, it has been difficult to verify for flat surfaces where equilibrium is hard to attain. Its extension to colloidal particles, especially colloids of low surface curvature, is partly justified by theory [42], but also strongly supported by experiments with proteins and micelles. Experimental tests of Eq (1) are more feasible with micelles because of their well-defined geometry, and because their surface charge density is uniform and can

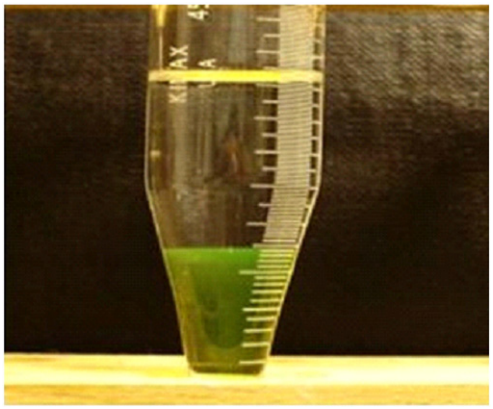

Fig. 2. Coacervate/supernatant after centrifugation of coacervate suspension System: BSA-F (bovine serum albumin labeled with fluorescein isothiocyanate) + poly(diallyldimethylammonium chloride) (PDADMAC), at pH 9.5 and I = 0.1 M NaCl [2].

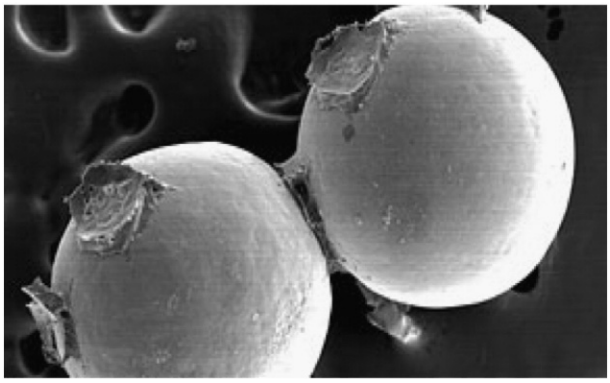

Fig. 3. Natural adhesive —the caddisfly larva glues formed by coacervates [23].

be adjusted by pH [43,24] or via the mole fraction of ionic surfactant in mixed ionic–nonionic micelles, "Y" [9]. For example, addition of anionic surfactant to a mixture of polycations and nonionic micelles results in progressive changes in micelle charge density, leading to transitions from noninteracting solutions to soluble complexes, at Y_c proportional to σ_c. In the case of proteins, the onset of noncovalent interaction with a polyelectrolyte is usually characterized by a slight increase in turbidity during acid or base titration, and this well-defined critical pH is attributed to the formation of soluble complexes at pH_c corresponding to Z_c. [2]. However, protein charge anisotropy complicates the interpretation of Z_c, relative to Y_c, and correspondence with theory is more difficult.

Non-uniform protein charge distribution ("charge patches") is revealed by polyelectrolyte binding on the wrong side of the protein isoelectric point [44]. Fig. 4 shows the possible conformations of such a polyanion bound to a positive charge patch. Due to charge anisotropy, Z_{eff}, which determines the interaction, is different from Z (total). Seyrek et al. concluded that the anisotropy of protein electrostatic domains determines the effect of ionic strength (I) on the binding of protein to a polyelectrolyte [45]. For example, a polyanion can bind to a positive domain of a globally negative protein.

Polyelectrolyte binding is different for micelles which have uniform surfaces (Fig. 5). Investigations of the critical binding condition for polyelectrolyte and oppositely charged mixed micelle revealed an average position of the bound polyion units from the micelle surface, which was obtained with appropriate potentiometric or fluorescence probe measurements. Potential decay curves for the micelle at conditions of critical Y and I all intersected at a single value of +5 mV, 0.6 nm from the micelle surface [47]. Since all critical conditions should have approximate binding energies = kT, this would imply a cooperatively binding polyion unit with an effective charge $Z \approx -5$. The real number of segments corresponding to an effective is unknown, but it is reasonable to imagine a sequence with contour length (5)(3 Å) = 1.5 nm, being accommodated close to a micelle with radius 3 nm. Beyond this distance, the charge of the PE "wings" plays an important role [49]. "Loop compliance" can stabilize the binding in PE–micelle systems. Kayitmazer et al. reported that the nonionic "wings" are more susceptible to long-range repulsion and less paired with the binding domain [49].

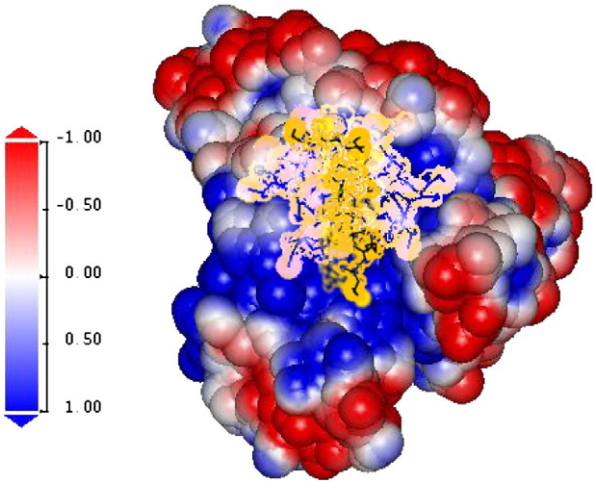

Fig. 4. Conformational freedom of charged decamer at its binding site on the protein, for pH 6.0 and I = 10 mM. Decamer is represented by orange atoms and black backbone. Red and blue correspond to negative and positive protein potentials, respectively, via solutions of the non-linear Poisson Boltzmann equation [46].

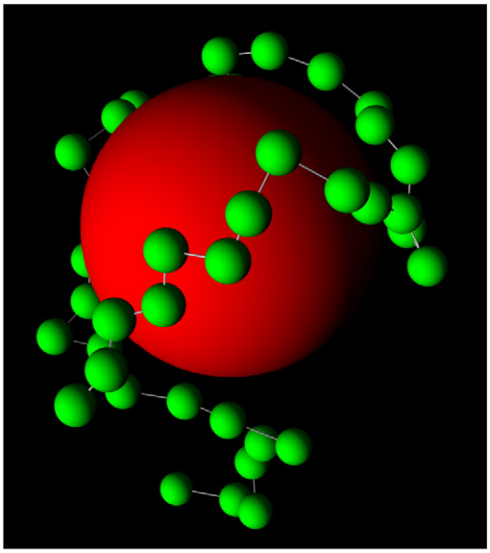

Fig. 5. Adsorption of a polyelectrolyte onto a spherical colloid surface [48].

2.2. Effect of ionic strength

Interactions between PE's and oppositely charged colloids are subject to screening by salt, although the nature of the salt dependence can be complicated by colloid charge anisotropy. High ionic strength I leads to dissolution of complexes. In the case of micelles, this can be compensated for by an increase in micelle charge density, Y. Therefore, in PE/micelle systems Y_c is shifted to larger Y values with added salt [8]. Similarly, in polyanion/protein systems, pH_c is generally shifted toward more acidic values in order to compensate the partial screening of the macroions [50]. Despite this similarity, the anisotropy of electrostatic domains around proteins play a dominant role in determining the ionic strength dependence of PE binding, particularly when binding is on the wrong side of pI. Seyrek et al. reported one consequence of protein anisotropy: a maximum in polyelectrolyte-protein affinity at ionic strengths corresponding to Debye radii on the order of the protein radius [45].

In 2.1, the ionic strengtital dependence polyelectrolyte-colloid affinity was expressed as κ^b. Values of b obtained by theory have been 3 [41], 11/5 [40] and 1 [34] for flat surfaces; while those for spheres and cylinders were reported as 1. However, the critical charge density for adsorption only increases by about 10% relative to flat surface [33,51]. b was obtained as a fitting parameter from salt dependence of σ_c for DMDAO micelles of different geometry. For spherical micelles, b was found as around 1.4, whereas for cylindrical micelles, b was around 2.0. Zhang et al. reported $b = 1.4$ for mixed micelles of carboxyl-terminated surfactants/nonionic surfactants and polycationic PDADMAC [52]. Experimental values of b for cylindrical micelles were closer to the theoretical values for flat planes of 11/5 [40] and 3 [41]. Not surprisingly, experimental values for colloidal particles of high curvature did not agree with any of theoretical results.

2.3. Effect of PE charge density

The dependence of σ_c on polyelectrolyte charge density can be expressed by $\bar{\xi}^a$. The charge per polymer repeat unit (q) which appeared in Eq. (1) is replaced by an average linear charge density ($\bar{\xi} = l^{-1}$) where, in order to include copolymers, l is the average distance between charges along the polymer backbone. Eq. (1) becomes

$$\sigma_c \bar{\xi}^a \sim \kappa^b \tag{2}$$

"a" was determined from the dependence of σ_c on $\bar{\xi}$ at constant b, where the values for b were obtained from log σ_c vs log κ plots of polymers with different charge densities. When $\bar{\xi}$ was varied through copolymerization of anionic (AMPS) and nonionic (AAm) monomers, (with l^{-1} taken from the average copolymer composition at different feed ratios or from the degree of sulfation of polyvinylalcohol (PVAS)), a was 0.6 for PVAS, and 0.2 for AMPS/AAm copolymers [53]. This was ascribed to the difference between $\bar{\xi}$ and an effective ξ (ξ_{eff}), which depends on the uniformity of charge distribution of the polymer, which would of course be most extreme for "blocky" polyelectrolytes, e.g. pectin [54,55] For PVAS, the uniform spacing of charged sulfate groups leads to ξ_{eff}/ξ close to 1, while the random composition of AMPS/AAm copolymers leads to $\xi_{eff} > \xi$ due to the presence of highly sulfonated pentads. The nature of the polyelectrolyte charge distribution might have a more complex effect on interactions with proteins whose charge heterogeneity introduces repulsive forces between polyanions and protein negative domains, and thereby alters the nature of the polyanion-binding site [49]. The surprising linearity between I and the net protein charge at the onset of binding was taken as evidence of the consistency of this binding site. Low protein binding of heparin, compared to AMPS25/AAm75, and AMPS80/AAm20, is due to the absence of nonionic residues in heparin which at pH>pI would reduce repulsive interactions between a bound PE sequence and negatively charged domains of the protein.

Critical conditions for the adsorption of a PE onto a colloid are influenced by chain flexibility and charge mobility [56]. As expected, increased binding was seen with a decrease in chain stiffness for three PE's with similar charge densities but different intrinsic persistence lengths, l_o: (1) AMPS25/AAm75, (2) hyaluronic acid (HA), (3) pectin. On the other hand, the more flexible poly(acrylic acid), exhibited weaker protein binding due to the repulsive forces between the polyanion and the negative charge domain of the protein. Lastly, stronger protein binding can arise from charge mobility: charge migration within a polyelectrolyte chain to form a sequence more favorable to binding than the statistically average sequence. Such "annealed" polyelectrolytes exhibited stronger binding than "quenched" polyelectrolytes.

2.4. Effect of PE molecular weight

The binding of mixed micelles of anionic surfactant sodium dodecylsulfate (SDS), and nonionic surfactant Triton X-100 to a positively charged polyelectrolyte poly(dimethyldiallylammonium chloride) (PDADMAC) was found to be independent of PE molecular weight (MW) for $3.00\times10^4<MW<4.28\times10^5$. PE MW does not influence pH_c for bovine serum albumin (BSA) and (PDADMAC) [9]. These results, along with the absence of any effect of PE concentration support the view of predominantly local electrostatic forces: involving a short sequence of PE segments [14,57].

2.5. Thermodynamics

Intrapolymer complex formation, soluble aggregate formation and coacervation may all have different thermodynamics. These different processes are often not well-resolved, and experimental results, especially calorimetric data, may reflect multiple events. For this reason, we discuss both binding and phase transitions in this section. PE-colloid stoichiometry is not fixed, e.g. the number of micelles or proteins bound per PE chain is variable; therefore binding equilibria are viewed via binding isotherms. Fitting the data to a selected multiple-binding model leads to values for binding site size (minimal PE occupancy region), number of binding sites, and intrinsic binding constants (k_b), the last quantity leading to ΔG^o. Thermodynamic quantities for coacervation can be directly deduced from calorimetry. Isothermal titration calorimetry (ITC) yields two results: ΔH^o for all processes taking place from over a range of stoichiometries (not model-dependent), and the binding isotherm (based on the assumption that measured enthalpies for each increment of added ligand reflect the extent to which that ligand is bound). When ΔG^o and ΔH^o are combined to yield ΔS^o, the different sources of these two terms need to be considered, if ΔH^o and ΔS^o are to allow for qualitative comparisons with proposed models.

Calorimetric measurements indicate that PE–colloid interactions, depending on conditions, can be exothermic ($\Delta H^o<0$) or endothermic, i.e. entropy-driven. Girard and coworkers [35] used ITC to determine the binding constant, stoichiometry, enthalpy, and entropy of β-lactoglobulin/low- and high-methoxyl pectin (β-lg/LM- and HM/pectin) complexes. They found that soluble intrapolymer complexation was enthalpy driven, whereas formation of soluble interpolymer complexes involved enthalpic and entropic factors. Harnsilawat et al. for β-lactoglobulin and sodium alginate at pH 3 and 4 found exotherms, due to the electrostatic binding of β-lg molecules to the sodium alginate; but at pH 4 and 5, they observed endotherms primarily due to dissolution of β-lg aggregates upon addition of sodium alginate to the cell [44]. Other studies have also shown successive appearance of an exothermic and endothermic signal, accompanied by phase transitions [58,59]. The more simple polyelectrolyte-micelle system, PDADMAC with SDS/TX100 micelles, did not exhibit any exotherms or endotherms but was found to have essentially no enthalpy change, indicating as do the endotherms mentioned above that both complexation and coacervation were mainly entropy-driven [60].

The complexation of PE's with an oppositely charged colloid is accompanied by a release of the condensed counterions that regain as much translational entropy as the free ones. Gummel et al. [61] reported the first direct experimental demonstration of counterion release in the lysozyme/poly(styrene sulfonate) (PSS) system using small angle neutron scattering (SANS) with specific counterion labeling, in which a significant scattering signal came only from counterions trapped in a shell of polyelectrolyte chains surrounding the complexes. The release of condensed counterions during complexation was accompanied by macroion charge neutralization. Skepo et al. studied interactions between a strong polyelectrolyte and spherical nanoparticles by Monte Carlo (MC) simulations [62], and demonstrated that counterion release was maximum at macromolecular charge equivalence.

While the, measurement of heat of binding by ITC is straightforward, the values of entropy or energy obtained are model-dependent. ITC analysis typically employs canned software (e.g. Microcal Origin) which (1) converts raw calorimetric data (heat evolved or consumed for each titration step, $\delta\Delta H^o$) to a binding isotherm, and (2) analyzes the binding isotherm to yield binding site number (size), and binding constant(s) from which ΔG^o and hence ΔS^o are obtained. The first step is based on the assumption that any decrease in $\delta\Delta H^o$ relative to its initial value is due to incomplete binding of the titrant molecules, as would be true for protein–ligand interactions. The second step is model dependent, typically involving the relationship between heat and protein/ligand molar ratio with either one or two binding sites. For the β-lg-pectin system, Girard and coworkers also treated the binding isotherms with the overlapping binding site (McGhee von Hippel) model [63], leading to a much higher number of binding sites and consequently lower binding constants than obtained with the "two sets of sites" binding model used for binding isotherms that show more than one inflection point [35]. The use of a two-site analysis in terms of two different steps might involve misapplication of a binding isotherm model. For polyelectrolyte-colloid systems, the binding model should be consistent with the protein as guest, not host. Analysis proceeding through steps (1) and (2), beginning with the raw data, is a prudent check on instrument software.

2.6. Size and structure of soluble complexes

Association in polyelectrolyte-colloid systems typically shows a series of sequential events involving (a) individual (non-interacting)

polymers or colloids, (b) primary (intrapolymer) complexes, (c) soluble aggregates, and (d) coacervates. Intrapolymer complexes consisting of one polymer chain decorated with colloids show radii similar to those of the polymer, i.e.15–30 nm. Interpolymer complexes "soluble aggregates" with radii ~50 nm or larger, are formed by the association of intrapolymer complexes. Such soluble complexes have been characterized by electrophoretic mobility [64], light scattering [11], turbidimetry [22], confocal laser scanning microscopy [65], small angle neutron scattering [66], Cryo-TEM [67], circular dichroism [68], and phase contrast microscopy [24]. Mekhloufi et al. studied the pH-induced structural changes during complex coacervation between β-lg and Acacia gum (AG, a.k.a. gum arabic) by the combination of different experimental techniques [69]. They characterized the phase transitions by monitoring turbidity and light scattering intensity under in situ slow acidification with glucono-δ-lactone. Above pH_c, R_h gradually increased above the value that corresponds to the R_h of AG alone observed for $pH<pH_c$. This was accompanied by an increase in turbidity and was attributed to the formation of β-lg/AG complexes, which coexist with free polyelectrolytes. On the other hand, Weinbreck and coworkers [50] reported for a similar system a decrease in complex size with increase in pH. At $pH>pH_c$ the initial radius of the complex is close to the radius of AG alone, while below pH_c, the radii of the complexes remain ca. 20 nm up to the point of phase separation [50]. Dubin and coworkers showed that soluble complexes of polyelectrolytes and mixed micelles (PDADMAC/TX100-SDS) close to the point of incipient complexation had sizes similar to that of the corresponding polymer [70,71]. The low compositional polydispersity of this system makes it possible to observe transitions from non-interacting state to intrapolymer complex, from intrapolymer complexes to soluble aggregate, and from soluble aggregate to coacervate.

3. Coacervation

In this section, we will discuss (1) the mechanism of coacervation, (2) the conditions for coacervation, and (3) coacervation models for coacervation of protein–PE and micelle–PE. For both protein–PE and micelle–PE systems, coacervation, induced by respectively pH or mixed micelle composition, is reversible and sharp, occurring within a change of ±0.1 in pH or ±0.02 in"Y". Thus, colloid-PE coacervation is a true liquid–liquid phase separation, broadened only by system compositional polydispersity [72]. Extensive heterogeneity with respect to both MW and composition, along with concentration gradients that can occur absent adequate mixing, obscure this fact in most studies of PE–PE coacervation. Additional evidence for the equilibrium nature of PE-colloid coacervation is the fact that the phase boundary does not depend on the variable used to enter the two-phase regions [73,9].

3.1. Mechanism of coacervation

3.1.1. Soluble complexes are precursors of coacervation

Studies indicate a hierarchy of structures consisting of PE-micelle primary (intrapolymer) complexes (apparent radius 15–30 nm) and clusters or aggregates (~50 nm or larger). PE-colloid coacervation arises from extended interactions among soluble complexes [24,10,74]. Upon gradual increase of colloid surface charge density, it is possible to identify different phase domains or regions, corresponding to either colloidal solutions or biphasic systems. Bovine serum albumin (BSA) and PDADMAC, originally free of interaction at low pH, start to form a primary (intrapolymer) complex at a critical pH, accompanied by a slight increase in intensity. Upon gradual titration by NaOH, an increase in BSA negative charge i.e., while net charge of the complex approaches electroneutrality, a second increase in or turbidity or a decrease in mean diffusivity indicates the aggregation of primary complexes [75]. This aggregation progresses up to the point of incipient coacervation which corresponds to the observation of coacervate droplets [24]. The transition from soluble complexes to aggregates is induced by elimination of transient regions that exhibit lower macroion charge compensation, i.e. polarization. The elimination of these regions in polyelectrolyte-colloid systems can be a driving force for colloidal association analogous to intermolecular dispersion forces.

3.1.2. Charge neutralization

For many systems coacervation tends to be maximum when the stoichiometry of the macroion charges is equal to one, which – ignoring counterions – corresponds to neutralization of the complexes [8,76]. For proteins, a gradual change of the pH allows the protein to begin to neutralize the charge on the polymer because of both an increase in protein charge and an increase in protein binding; therefore, the charge of the complex can approach electroneutrality. This promotes higher order association and, finally, phase separation. Experiments with polyelectrolyte-micelle systems showed that the maximum turbidity in the coacervation region with respect to "Y" corresponds to zero mobility and maxima in soluble aggregate size. However, the coacervation region of polyelectrolyte-micelle system (and polyelectrolyte complex systems in general) is broader than the exact point of electroneutrality. This non-stoichiometric coacervation was explained by Shlovskii et al. [77]. They predicted that the polyanion host and polycation guest could form a neutral macroscopic drop by intracomplex or intercomplex disproportionation when the macroion charge stoichiometry deviates from unity. Inter-complex disproportionation involves migration of some polycations to make some complexes neutral. Thereupon, neutralization facilitates condensation into a macroscopic drop while other complexes become even more strongly charged. In intra-complex disproportionation, polycation migration leads to the formation of "micro-droplet", a partially neutralized soluble aggregate in which excess charges are relocated to a distal region or "charged tail". This theory accounts for the occurrence of stoichiometric and nonstoichiometric coacervation even in systems of low compositional polydispersity.

3.2. Conditions for coacervation

3.2.1. Ionic strength

Critical conditions for the onset of coacervation, defined as pH_φ and Y_φ exhibit strong ionic strength (I) dependence. An increase in I requires a concomitant increase in macroion attraction to overcome screening. Therefore, one would expect a monotonic dependence of pH_φ on ionic strength; however, the pH_φ vs I phase boundary for BSA/PDADMAC demonstrated both entrance into and exit from the coacervation region by addition of either salt or water [73]. This nonmonotonic ionic strength dependence, with coacervation occurring most readily at 20 mM NaCl, was reminiscent of the maximum in the binding constant at $I = 20 \pm 10$ mM for BSA and a hydrophobically modified polyacrylic acid, attributed to protein charge anisotropy [45]. Recently, Xu et al. explained how non-monotonic behavior of pH_c could lead to nonmonotonic behavior of pH_φ [78]. pH and I alone determine the local protein-polyelectrolyte electrostatic affinity which governs the number of proteins bound per polymer chain, n. On the other hand, pH_φ involves also long-range inter-complex interactions that can be controlled by the net charge on the soluble complex, which (neglecting counterions) is $Z_T = Z_P + nZ_{pr}$, where Z_P and Z_{pr} are polyelectrolyte and protein charge. The condition for coacervation, $Z_T = 0$ requires that Z_P and Z_{pr} are of opposite sign and n is sufficiently large. A decrease in n can result from screening of short-range PE–protein interaction, at high I, and repulsion between nearby bound proteins at low I. The requisite increases in Z_{pr} are identical to requisite increases in pH_φ and hence a minimum in pH_φ with respect to I. Similarly, coacervation in the polyelectrolyte/mixed micelle

system can be both enhanced and suppressed by changing salt concentration through changing the number of bound micelles [8].

3.2.2. Stoichiometry

Stoichiometry refers to both the mixing ratio of colloid:polymer, r, and the ratio of colloid:polymer within the complex or coacervate, r^*. These "bulk" and "micro" stoichiometries, of course, need not be the same since free colloids or free polymers may exist in the case of weak binding or when one is in excess. Liquid–liquid phase separation (coacervation) can occur when the combined contributions of all ionic species, including small ions, allows for the formation of neutral or near-neutral aggregates. For high charge density polyelectrolytes, and particularly in the absence of salt, charge-neutral, counterion-free precipitates form when bulk stoichiometries $([+]/[-]_{bulk}) = 1$. This is the basis of "colloid titrations" [79]. Even in the presence of salt, the binding isotherm ensures that n (colloid particles bound per PE chain) will increase with r (up to saturation). Consequently, an increase in r leading to an increase in n can lead to enhancement or suppression of coacervation. pH_φ is strongly r dependent, because an increase in r would usually correspond to an increase in n, which as noted above lowers pH_φ when protein is bound to a polycation. While the PE:colloid combining ratio is evidently not constant, a type of stoichiometry can emerge when the biphasic species (precipitate or coacervate) uniquely contain equal positive and negative macroionic charges. This is most likely when a high degree of ion-pairing is expected, corresponding to a level of charge symmetry, "quenched" (pH-independent) charges and low ionic strength, e.g. as for the counterion-free "scrambled polysalts" of Michaels et al. [80,31]. Even when these conditions are not met, charge neutrality can be observed electrophoretically at the point of maximum coacervation: the electrophoretic mobility of the complexes converges to zero, while the turbidity passes through a maximum indicating a maximum molecular mass for soluble complexes [8]. Such stoichiometric complexation corresponds to a fixed compositional ratio (microscopic ratio), a large binding constant and well-defined products. Usually, the compositional ratio of the coacervates is different from the mixing ratio, r, since small ions are involved in the charge balance; i.e. $r \neq r^*$. Below charge neutralization complexes are soluble; beyond charge neutralization point, excess charge can dissociate complexes. Entry into and exit from coacervation with stoichiometry is exhibited in many systems: Pectin and β-lactoglobulin [81], lysozyme and sodium polystyrene sulfonate [82], gum Arabic and chitosan [83], PDADMAC and BSA [73].

3.2.3. Temperature

Kaibara et al. [24] saw no temperature dependence for pH_c and pH_φ [84] for PDADMAC and BSA. On the other hand, because coacervation of PE/micelle system can be entropy-driven, by release of counterions, temperature can induce coacervation. Temperature can affect micelle size [85], but this does not preclude a true phase transition that is marked by an abrupt increase in turbidity at T_Φ, subsequent to formation and growth of soluble complexes. The transition becomes more sharp when polydisperse surfactants (Triton X-100, TX100, and commercial dodecyl octa(ethylene glycol) monoether, $C_{12}E_8$,) are replaced by monodisperse $C_{12}E_8$ [86]. Upon heating of the coacervate itself, a second transition is observed, and a new coacervate and supernatant are obtained at T_φ'. This phase transition in the coacervate has been characterized by turbidimetry [87], dynamic light scattering and rheology [88], and transition can also be accomplished by shear.

3.2.4. Shear

Dubin et al. reported shear-induced phase separation at a temperature close to but below that for quiescent phase separation [87], was the first report of shear induced phase separation in polyelectrolyte-colloid systems. Once a critical temperature range and/or shear rate is achieved, the fluid exhibits shear-thinning coupled with phase transition [88]. As illustrated in Fig. 6, shear flow transforms the polyelectrolyte-micelle complexes into extended chains or "necklaces of polyelectrolytes decorated with micelle beads" [89]. These extended chains allow efficient intercomplex interactions, which promote the expulsion of small ions from the complex, another mechanism for phase separation. This phenomenon, observed by turbidity and by viscosity, indicated a connection between shear and temperature induced phase separation (Fig. 6). Most studies in PE/protein systems, investigated the effect of shear or shear rate on the size of coacervate droplets or the coalescence of coacervate suspensions. It has been shown that the size of the coacervate suspensions decreased with the increase of the shearing rate, while at a constant shearing rate, the size of the coacervate suspensions increased [90].

3.3. Models of coacervation

While coacervation comprises a sequence of events, the extant models focus only on one or two of them. Perhaps the most conceptually simple is the "colloid model" which views the objects susceptible to phase separation as soft colloidal particles, and considers only their number concentration and interaction potentials, disregarding equilibria among the macromolecules or aggregate precursors. Conversely, the "condensation" model of Shlovskii allows the system to reach the point of coacervation by disproportionation, so the resultant coacervate ("condensate") is likely to comprise subunits different from the objects remaining in the dilute phase [77]. System compositional polydispersity provides a more heterogeneous array of macroions to select from for condensation, adding an additional dimension to disproportionation. Chain length polydispersity in particular is considered in the classical coacervation models of Overbeek [4] and Veis [91] which also take into account contributions of chain configurational entropy during structural rearrangements. Veis more recently [32] considered the related question of the retention of complex *structure* during such rearrangements in which complex *stoichiometry* is preserved. However, none of these models allow for the redistribution of counterions as part of complex reorganization; evidence for this can be inferred from characterization of polyelectrolyte-protein coacervates which we will present as an extension of the condensation model. For these systems, restructuring may be more evident.

3.3.1. Soft colloids with short-range attraction and long-range repulsion (SALR)

Here, the dense and dilute phases differ only in the concentration of particles. These "soft colloids" should correspond to the objects present at incipient phase separation; they may in fact be "clusters" of somewhat uniform complexes. In this model, coacervation occurs when the net attraction energy among clusters overcomes the loss of

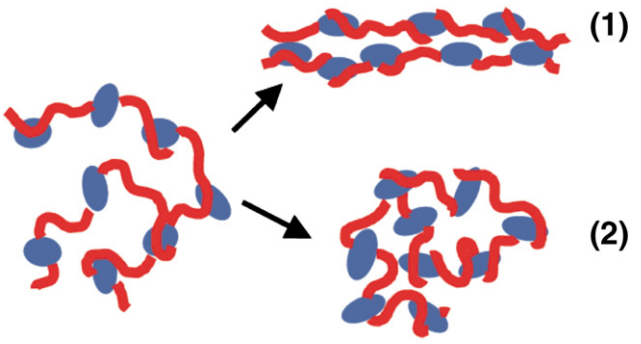

Fig. 6. Schematic representation of (1) shear- and (2) temperature-induced phase separation for PDADMAC/TX100-SDS coacervate. Both processes involve loss of counterions arising from increased polyelectrolyte-micelle interactions, but by an intercomplex vs intracomplex mechanism for the former [88].

entropy, or at a sufficiently large cluster volume fraction. The structure of the dilute phase clusters depends on the charge of their precursor complexes. Neutral complexes readily attract via both enthalpic polarization effects, and entropic effects related to increased chain configurational entropy in a random structure [91]. The growth of clusters from charged soft colloids is subject to long-range "coulomb blocking" which introduces a second length scale, a characteristic maximum cluster size that will be retained in the dense phase [92,93]. Stradner et al. provided the first experimental confirmation that a combination of short-range attraction and long-range repulsion (SALR) results in the formation of small equilibrium clusters of lysozyme molecules [94]. Similarly, consideration of SALR in Monte Carlo simulations by Archer and Wilding showed the presence of dilute suspension of mesoscopic clusters, and/or a dense suspension of primary particles having mesoscopic void-like domains [95].

More relevant to the inter-macroionic complexes considered in this review, Gummel et al. studied turbid suspensions (i.e. metastable mixtures of dense and dilute phases) formed by complexation of sodium poly(styrenesulfonate) (PSS) with lysozyme [96]. From contrast matching SANS they observed, for bulk charge stoichiometry $[-]/[+]>1$, dense electrically neutral ca. 15 nm protein–PE cores (or "primary complexes"), surrounded by more dilute polyelectrolyte-rich "coronas". The dense domains persisted but coronas were absent for the case of ($[-]/[+]<1$), with excess protein segregated in the dilute phase. All samples showed a 2.1 fractal dimension of the cores as expected for reaction-limited colloidal aggregation (RLCA), i.e. limited by a repulsive potential barrier. In addition, freeze-fracture electron microscopy (FFEM) pictures were very close to TEM pictures obtained for other colloidal systems aggregated by RLCA [97] (Fig. 7). In this way, Gummel at al provided a kinetic view of SALR controlled aggregation (as opposed to clustering) of "primary complexes" of PSS and lysozyme formed by coulomb blocking. (See Section 4).

While treating the objects present at incipient phase separation as colloids makes it possible to represent the observed states with phase diagrams, these objects present here represent complex structural hierarchy, being formed from soluble aggregates which in turn arise from unlike macroions (the hierarchy extending to even lower length scales for micelles of surfactant molecules). Such opportunities for compositional polydispersity, disproportionation and polarization are difficult to represent in the colloid model. The attendant equilibria among complexes, constituent low molecular weight species and ions are all subject to effects of e.g. ionic strength, surfactant composition, polymer MW and temperature in ways not readily accounted for in the colloid model. That coacervation itself can influence these equilibria is taken into account by models in which the organization and stoichiometry within the coacervates differ at many length scales from those in the dilute phase. Models which explicitly recognize soluble complexes as coacervate precursors more readily accommodate system compositional polydispersity and polymer chain entropy.

3.3.2. "Veis" Symmetrical Aggregate Model

In the Voorn–Overbeek theory [98,99], the spontaneous formation of a concentrated coacervate phase is driven by a gain in electrostatic free energy at the expense of a decrease in mixing entropy. This model assumes (i) negligible solvent–solute interactions, (ii) the absence of site-specific interactions, and (iii) the absence of soluble complexes [4]. Since previous studies on the polyelectrolyte-micelle systems show the existence of the soluble complexes and soluble aggregates thereof, we turn to the model of Veis et al. [91] who modified the Voorn–Overbeek equations for complex coacervation and concluded that this occurs in two steps: (i) interaction of oppositely charged polyelectrolytes by electrostatic interaction to form complexes (referred to as "aggregates", a term we reserve for soluble species with more than two macroions) of low configurational entropy, and (ii) re-arrangement of these complexes to form coacervate in equilibrium with the dilute phase [91]. If bulk stoichiometry does not coincide with local charge neutrality, the macroion in excess can remain in the dilute phase, and this "segregation" to attain complex neutrality can be amplified by system compositional polydispersity. This rearrangement might decrease chain entropy (chains are more ordered in coacervate than in one-phase), increase chain entropy (chains more disordered in coacervate), or have no effect on chain entropy, Veis proposes the second case. Accordingly, while 1:1 soluble complexes can only approach neutrality given some sort of symmetry with respect to chain length and charge density, more options exist for large multipolymer complex with adjustable stoichiometry (i.e. soluble aggregate) particularly in polydisperse systems. In this way, more macroions can be incorporated into the coacervate. In Veis' description of "random" coacervates, all trace of such multipolymer complexes should disappear via random mixing.

More recently, Veis considered the presence of symmetrical aggregates that might differ in chain length, or excess charge density. The mixtures of the polyions at non-equivalent concentrations led to two possible models, where (a) dilute and coacervate phases both contain the symmetrical aggregates, and any excess of one polyion or the other, or (b) the symmetrical aggregates are found only in the dilute phase, while the coacervate phase was randomly mixed. The

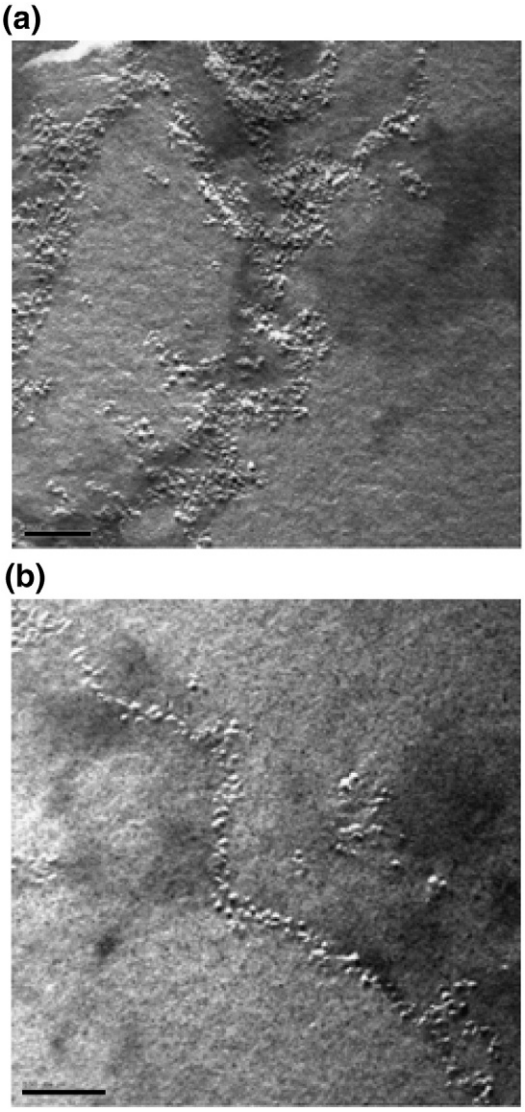

Fig. 7. TEM picture after freeze-fracture at intermediate resolution for the $[-]/[+]_{intro}=1.66$ sample. Bar = 100 nm (1000 Å). (a) Dense areas of primary complexes structures and (b) wires of primary complexes structures [97].

dilute phase, with stoichiometry more biased toward the macroion in excess, may still be susceptible to further coacervation if an intensive variable such as pH or ionic strength provides an additional impetus for coacervation. Progressive depletion of dilute phase macroions in this way may be analogous to MW fractionation of polydisperse polymers by reduction in solvent affinity via e.g. temperature. In the Veis model, the ionic strength is considered primarily as a determinant of complex stability (tendency to resist dissociation), while the enhancement of coacervation by temperature arises from the positive entropy of chain mixing in coacervation. The absence of counterions in the Veis model probably neglects an important contribution to the entropy of coacervation.

3.3.3. Shklovskii's Condensate Model

Shklovskii's condensate model pictures charge segregation ("disproportionation") on a more intimate (e.g. intrapolymer) length scale; Veis' "Symmetrical Aggregate Model" allows for expulsion of excess macroion into the dilute phase, and Gummel et al. indicate expulsion of excess polyanions into a "corona", The incorporation into dense phases of complexes without charge stoichiometry can be accomplished by many different types of rearrangements. According to Shklovskii et al., the polyanion and polycation most readily form a neutral macroscopic drop ("condensate") when the bulk stoichiometry [+]/[−] equals 1. Near [+]/[−] = 1, there can be coexistence between neutral drop and free chains in excess (segregation), or intracomplex or intra-cluster disproportionation by formation of "tadpoles" with a neutral part and a charged tail (Figs. 8 and 9). While Veis recognized soluble complexes as coacervate precursors, the Shklovskii model more explicitly accommodates clusters (multipolymer aggregates). In this disproportionation model, the excess would be complexes or aggregates; as shown in Fig. 9, the excess in the Veis (segregation) model are individual macroions. The formation of neutral droplets is favored by correlation energy – energy gained by the orderly arrangement of positive and negative charges in the drop – among the multipole-like clusters. The repulsions among clusters of equal net charge can be screened by addition of salt, which broadens the coacervation domain [8,77]. The release of counterions, not considered in the Zhang & Shklovskii model [77], provides additional favorable entropy for the merging of clusters. In the colloidal model, all of these effects would be included in the interparticle interaction energy. *Local* release of counterions can, in addition, provide net charge balance for otherwise uncompensated macroions in regions of coacervated clusters. This has been discussed by Gummel et al. [100] whose studies revealed that the macroion in excess, in this case the polyelectrolyte, is locally segregated in the corona along with its counterions. The electrostatic association in the core is exenthalpic; the unfavorable chain entropy in the restricted protein-polyelectrolyte core is relieved by the entropy of expulsion into the corona of the excess polyelectrolyte counterions. The model proposed by Gummel et al. might be considered as an extension of Zhang and Shklovskii with excess polyelectrolytes (and their counterions) expelled to a dilute *meso*phase, i.e. the condensed state representing the result of clustering of complexes subject to intracomplex disproportionation (Fig. 9c).

While several parameters are neglected in one or more of the models mentioned, ionic strength is considered by all models. According to Veis ionic strength dissociates aggregates. In the Colloid Model with SALR, high ionic strength shifts the balance in favor of attractive interactions by screening electrostatic repulsions. This behavior is repeated in the Shklovskii Model, which also predicts complex growth with *I*. The colloid model predicts fewer but larger aggregates at low temperature, while Veis predicts gelation at high temperature. Only the Veis model considers compositional polydispersity: an increase in temperature leads to the coacervation of different polymer fractions.

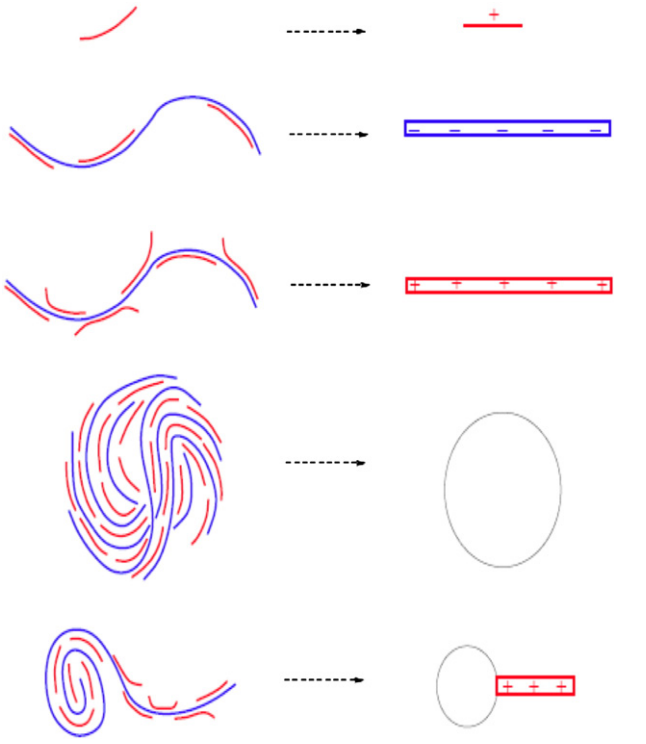

Fig. 8. Objects appearing in a solution of a long polyanion (PA) and a short polycation (PC): (a) a single PC, (b) negative PA–PCs complex, (c) positive PA–PCs complex, (d) condensate of almost neutral complexes and (e) tadpole made of one PA–PCs complex. Here, only the case of positive tail is shown. The tail can also be negative [77].

Therefore, the yield could be obtained at different temperatures unless the system is too concentrated. The disappearance of coacervation at very concentrated system is called "self-suppression" by Veis. This concentration dependence is also taken into account by the colloid model in terms of polymer depletion effect, which will be enhanced by increase of concentration; therefore, the clustering will be facilitated. Shklovskii Condensate Model accounts for the phase separation with the system whose charge deviates from zero. In this model, the system consists of two oppositely charged polyelectrolytes whose charges cannot vary and the compositional polydispersity has not been considered as discussed above. If polydispersity is incorporated in this model, we would adapt this theory by considering the micelle composition polydispersity and thereof, complex composition polydispersity since the micelles' charge can be varied by the Y value as discussed earlier. Therefore, the compositional distribution for ionic/nonionic mixed micelles can lead to disproportionation among micelles, which facilitates the exchange of micelles of different Y among complexes to make them attain charge neutrality and thus phase separate.

3.4. Structure determination in complex coacervates

In this section, we will present our results of imaging (fluorescence microscopy, Cryo-TEM), scattering (SALS, SANS), diffusion (FRAP, PFG-NMR, DLS), and rheology experiments to understand the structure of micelle–PE and protein–PE coacervates. Structure determination for soft matter of irregular structure and low contrast between its components cannot be trusted solely on imaging, which is prone to artifacts. Thus, we have utilized both direct and indirect experimental methods to reach a final model of the coacervate structure, which is neither regular nor homogeneous.

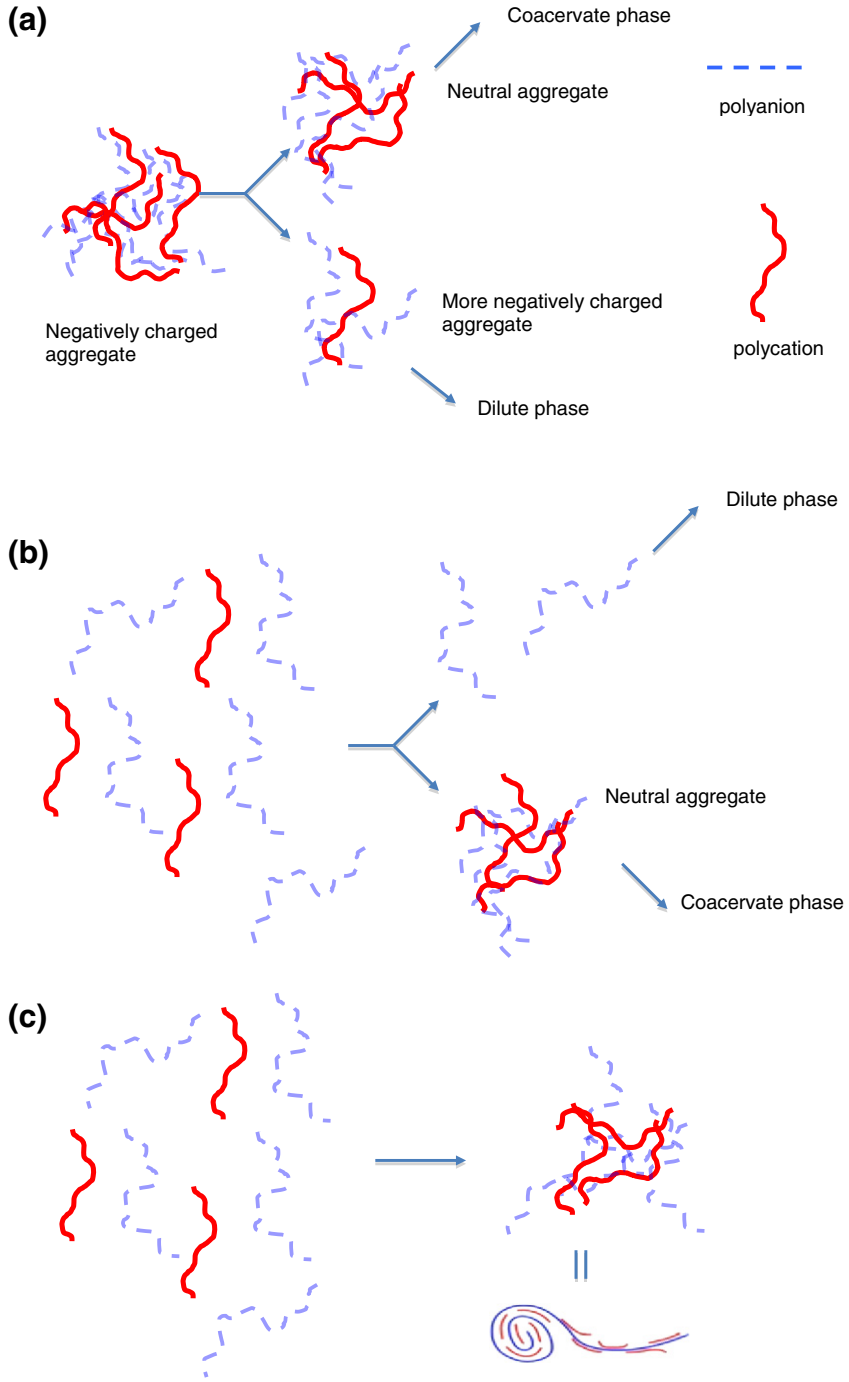

Fig. 9. Scheme to describe (a) intercomplex disproportionation, (b) segregation and (c) intracomplex disproportionation leading to formation a tadpole taken from Ref. 77 (see Fig. 8).

3.4.1. Imaging of coacervates and coacervate suspensions

Imaging of complex coacervates has helped to develop models to explain the structure of coacervates and coacervate suspensions, at the meso- and micro-length scales, respectively (Fig. 3).

3.4.1.1. Fluorescence microscopy of PDADMAC-BSA coacervate suspensions. Fluorescence microscopy of a coacervate suspension of PDADMAC with BSA and BSA-F (BSA labeled with fluorescein isothiocyanate) revealed micron-sized spherical coacervate droplets (Fig. 10) [101], similar to e.g. the SEM images of albumin/acacia coacervate suspensions [102a] or optical microscopy images of gelatin-gum Arabic coacervate suspensions [102b]. It was also interesting to find that the size distribution of the BSA/PDADMAC microdroplets was narrow at neutral pH (pH~7) but broadened with an increase in larger droplets at higher pH's; i.e. pH = 9.0 [101].

3.4.1.2. Cryo-TEM of protein–PE coacervates. Application of cryogenic-transmission electron microscopy (Cryo-TEM) to the study of PDADMAC-BSA coacervates has provided images of higher resolution without the need for labeling. Cryo-TEM images [75] obtained at high electrostatic interaction conditions (pH = 9, I = 50 mM NaCl) demonstrated a random distribution of irregular and partially

interconnected solid-like regions of protein-rich domains ("clusters" or "dense domains") with interdomain distances of 300–700 nm (Fig. 11a). Some of these solid-like regions have sizes similar to those of desolvated intrapolymer complexes ("aggregates"), i.e. 50–100 nm, while the rest are between 100 and 1000 nm. Although these aggregates also appeared at a weaker interaction strength; namely, pH = 8.5 and I = 100 mM NaCl, connections among the aggregates were more fuzzy, but one can easily imagine a tendency of these aggregates to form linear arrays [30] (Fig. 11b).

3.4.1.3. Cryo-TEM of micelle–PE coacervates. Earlier Cryo-TEM images (Fig. 12) of micelle-polyelectrolyte coacervates demonstrated a continuous interconnected network of micelle-rich domains [13]. Follow-up studies [88] focusing on the effect of temperature on coacervation have found that phase state of the system depended on the magnitude of the difference between the Cryo-TEM vitrification temperature (T_{vitr}) and the second phase separation temperature (T_φ') encountered when the coacervate is heated. A critical temperature of T_φ' might also induce an additional phase separation for optically clear micelle–PE coacervates. When the T_{vitr} is close to T_φ', an extended cluster structure of interconnected aggregates is again observed (Fig. 13b). On the other hand, when vitrification takes place above T_φ', one observes disconnected clusters (Fig. 13a) reminiscent of the structures of protein-polyelectrolyte coacervate in Fig. 11(b). The commonality of the two systems is the level of desolvation which accompanies counterion expulsion, induced by high pH for the protein–PE system, and elevated temperature for the micelle–PE system. In both cases, the sizes, ca. 30–50 nm, are within the range of soluble complexes or aggregates thereof, and likely reflect partial collapse of these species.

3.4.2. Small-angle light scattering (SALS) of micelle–PE coacervates

Micelle–PE coacervates of the PDADMAC-TX100/SDS system go through a second phase separation when subjected to shear or elongational flow at temperatures between T_φ and T_φ' [88]. Two-dimensional small-angle light scattering (SALS) was used to observe temperature and shear-rate related size changes at length scales, 0.94–5.0 μm. At low shear rates and low temperatures, SALS images are almost black due to the absence of scattering. At a critical temperature and shear rate, scattering from circular microdroplets arises, which indicates the onset of anisotropic phase-separation. As the shear rate is increased, microdroplets transform from circular to ellipsoidal shapes in the direction of the flow. In the shear-rate range of 0.1 to 25 s^{-1}, the droplet size and the aspect ratio varied from 1 to 4 um and 1 to 4, respectively. Similar changes in size and shape of the droplets were observed as temperature is raised at a constant shear rate (Fig. 14).

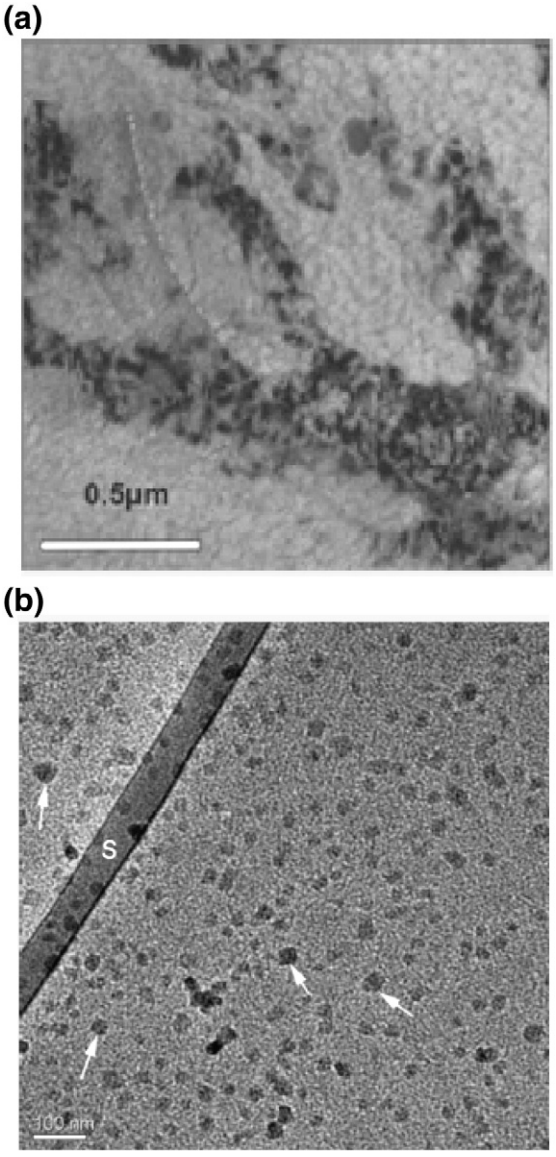

Fig. 11. Cryo-TEM image of BSA-PDADMAC coacervate prepared at a) pH = 9.0, I = 50 mM NaCl [75] b) pH = 8.5, I = 100 mM NaCl. "S" denoted the support film. The scale bar is 0.1 μm [30].

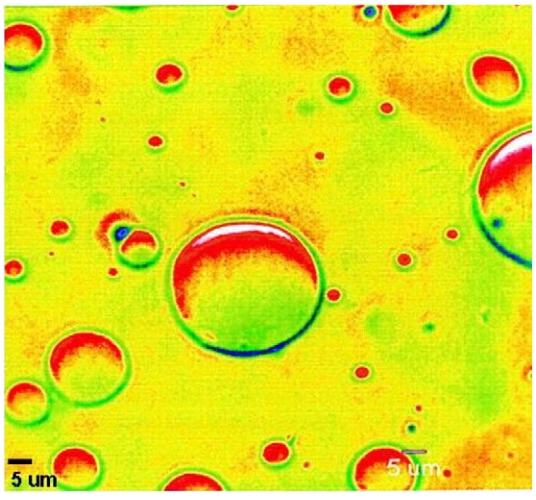

Fig. 10. PDADMAC-BSA coacervate suspension prepared at pH 9.0, I = 0.1, r = 5, C_p = 0.1 g/L. The scale bar is for 5 um [101].

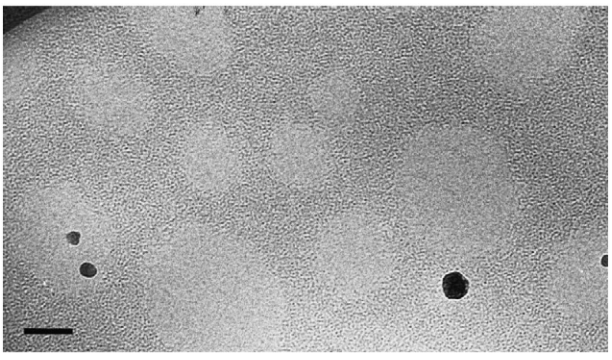

Fig. 12. Cryo-TEM image of PDADMAC/SDS-TX100 coacervate prepared at Y = 0.37, I = 0.4, C_p = 2 g/L. Bar = 100 nm [13].

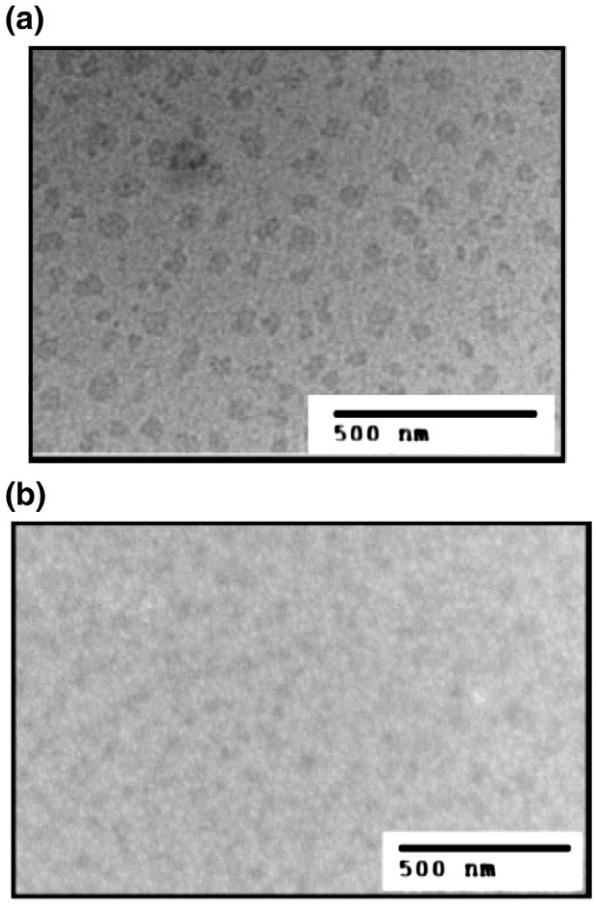

Fig. 13. Cryo-TEM image of PDADMAC/TX100-SDS coacervates prepared at (a) Y = 0.37, C_p = 2 g/L, I = 400 mM NaCl, T_φ = 12 °C, T'_φ = 22 °C; (b) Y = 0.35, C_p = 3 g/L, I = 400 mM NaCl, T_φ = 19 °C, T'_φ = 24 °C. Vitrification temperature was 24 °C for both cases [88].

3.4.3. Colloidal and PE diffusion in coacervates

Measurement of diffusivities within coacervates provides an indirect way to confirm the micro- and meso-scale structures observed by the imaging techniques. We have employed three different techniques for this purpose: 1) Dynamic light scattering (DLS) provides information about the apparent mutual diffusivities, which are dominated by the colloids (proteins and micelles) due to their scattering, relatively stronger than polyelectrolytes. 2) Fluorescence recovery after photobleaching (FRAP), on the other hand, gives information about the average diffusivities of the fluorescently tagged macromolecules. Thus, the diffusivities strictly belong to the labeled probes; BSA and a neutral polysaccharide of the same size. 3) Pulsed-field gradient NMR (PFG-NMR) can be tuned to the signal from the polyelectrolytes and thus probe the assembly of the polyelectrolytes within the coacervate.

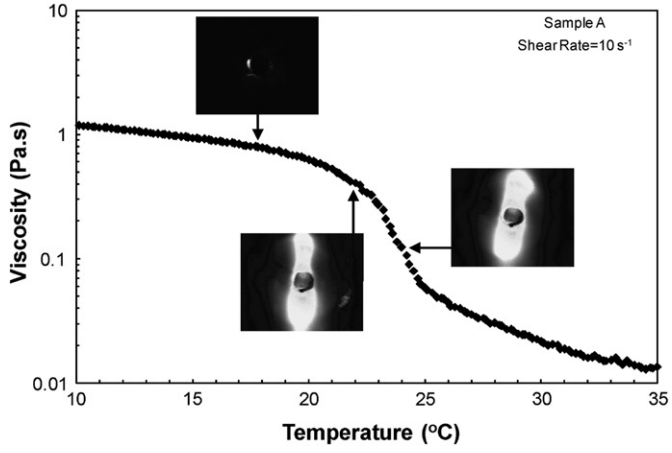

Fig. 14. Viscosity as a function of temperature at a shear rate of $10s^{-1}$ for PDADMAC/TX100-SDS coacervate prepared at Y = 0.37, C_p = 2 g/L, I = 400 mM NaCl, T_φ = 12 °C, T'_φ = 22 °C. Arrows point to the locations of the aforementioned SALS images [88].

3.4.3.1. Diffusivities of the colloid in the coacervates. DLS of both protein-polyelectrolyte [30] and micelle-polyelectrolyte [87] coacervates has displayed a distribution of multiple apparent diffusivities, with unexpectedly high fast mode diffusion coefficients. According to the Stokes–Einstein theory, it is expected that the fast mode diffusivities should vary linearly and inversely with increase in the viscosity of the medium. However, Stokes–Einstein theory assumes a homogeneous fluid. The unexpectedly high diffusivities suggest that the fast mode belongs to the colloids (proteins or micelles) whose motions are relatively unconstrained in the dilute domains within the coacervates. For PDADMAC-BSA coacervates, the DLS fast mode is independent of temperature and polymer molecular weight but is linearly dependent on pH. The monotonic increase in the amplitude of the fast mode with pH is accompanied by more solid-like (longer relaxation time, non-translational mutual diffusion). This suggests a compaction of the dense domains along with less constrained dilute domains (Fig. 15). For Chitosan-BSA coacervates, there are two fast modes (Fig. 15). The more narrow range of diffusivities with chitosan may indicate the absence of contracting dense domains and concomitant vacation of dilute regions. This might be a reflection of weaker interactions in the chitosan case, for which the charge density of the polymer is less than half that of PDADMAC, while the protein charge at pH 5.8 is far less negative than at pH 9.

DLS slow modes are related to the dense domains within the coacervates. The diffusive, angle-independent, slow mode (S1) is attributed to the protein or micelle diffusion within the dense domains. The slowest mode (S2), which is non-diffusive (angle-independent), is correlated with the relaxation time (lifetime) of the dense domains. At strong electrostatic interaction conditions, dense domains have longer relaxation times; therefore, more stable. The three orders of magnitude increase in the lifetime of Chitosan-BSA coacervate indicate a different mesophase structure.

Complementary to DLS results, FRAP gave insights about the mesophase structure of coacervates at longer length and time scales (Fig. 16) [75]. Diffusion coefficients of a neutral probe, Ficoll-isothiocyanate (Ficoll-F), in PDADMAC-BSA coacervates were compared to those in a concentrated solution of dextran with the same macroviscosity. The faster diffusion of Ficoll-F in coacervates than in an entangled dextran network reaffirmed the presence in the coacervate of partially interconnected (non-isolated) regions of low effective viscosity.

FRAP results for Ficoll-F diffusion could be resolved into fast and slow modes: These two modes were compared to the modes in DLS. Diffusion coefficients for Ficoll-F (from FRAP) and for BSA (from DLS) converged at most of the pH range studied. At the shorter length scale of DLS, a probe would follow a path not obstructed by dense domains. At the long length scale of FRAP, diffusivities would be slowed down due to the presence of obstacles. However, these dense domains only constitute 15% of the whole coacervate volume. Thus, they are too isolated to slow down the diffusivities, which indicate free or unhindered Brownian diffusion.

Slow mode diffusivities of Ficoll-F (FRAP) are larger than BSA (DLS). As mentioned above, DLS slow modes correspond to diffusion within dense domains. However, at time scales longer than DLS diffusive (angle-dependent) relaxation times, dense domains can break up before reassembling again. During this process, a probe molecule would then easily transit the broken domains. The FRAP set-up easily captures these dense domain dissolution effects, which depend on the strength of

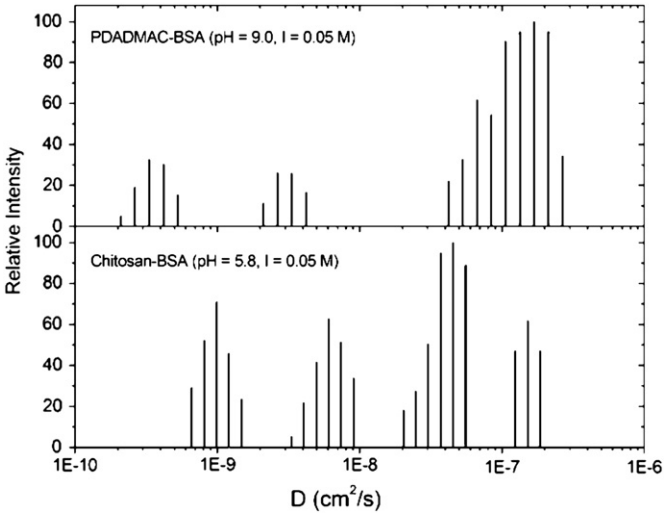

Fig. 15. Relative intensity vs. apparent *D* for coacervates prepared with PDADMAC-BSA and chitosan-BSA. The values in parentheses are the conditions used to make the coacervate [30].

electrostatic interaction. At high pH and low salt, conditions of high charge for BSA, FRAP diffusivities decreased due to increased tortuosity in the pathway of Ficoll-F diffusion. Whether the high tortuosity is a result of the increased interconnectedness of dense domains or an increase in their lifetimes requires additional imaging experiments. Lastly, Ficoll-F was replaced with FITC labeled BSA (BSA-F) in the experiments to examine the effect of an interacting probe on fast and slow modes. However, FRAP could not resolve these modes but could only give average diffusivities for BSA-F. Thus, it was concluded that electrostatic adsorption at dense/dilute domain interfaces leads to an intermediate mode.

Aside from electrostatic interaction-related parameters, temperature is an important factor for diffusivities within coacervates, especially when the colloid is a micelle. At temperatures higher than the temperature for the onset of aggregate formation within coacervates itself; i.e. $T>T_{\varphi}'$, apparent fast mode diffusivities (D_{fast}) increase sharply for the PDADMAC/TX100-SDS system [87]. The abrupt increase in D_{fast} suggests a less hindered diffusion for micelles in the dilute domains. This interpretation agrees well with the Cryo-TEM image above (Fig. 13a), which indicates disruption in the interconnectivity of the dense domains at higher temperatures.

Reorganization of the dense domains is also evidenced by a minimum in the slow mode diffusion coefficients and a maximum in the scattering intensities at 25 °C. The decrease of D_{slow} at T<25 °C indicates higher effective microviscosities within the dense domains as a result of their desolvation. As temperature is increased beyond 25 °C, contraction of dense domains is accompanied by a larger total area of dense/dilute domain interfaces. These interfacial areas provide a less constrained platform for exchange of micelles between the two domains; thus, the increased diffusivities.

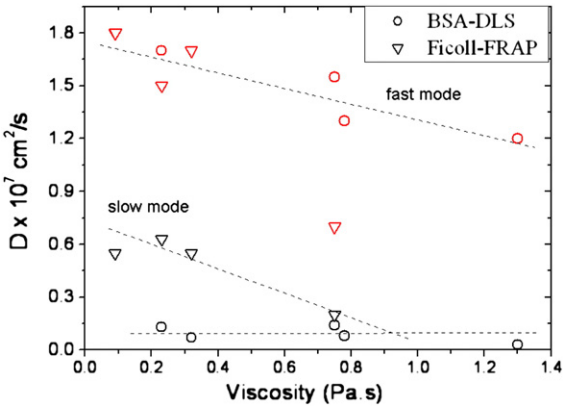

Fig. 16. Apparent diffusion coefficients vs. macroviscosity for Ficoll-F in coacervates as measured by FRAP; and BSA in coacervates as measured by DLS (Figure adapted from [75]).

3.4.3.2. Polyelectrolyte diffusivity within the protein-polyelectrolyte coacervates. PFG-NMR with a specific stimulated echo sequence could distinguish the diffusion data of polyelectrolytes from proteins in the PDADMAC-BSA coacervates [103] and so give insights into PE self-assembly. Three different diffusional modes, i.e. fast1, fast2, and slow, were recorded for PDADMAC in the coacervates prepared for a certain pH, I, and polymer MW (Fig. 17). Resolution of diffusion coefficients into three different modes, instead of a weighted average diffusion coefficient, enabled to analyze mobility events in each microviscosity region separately. The slowest diffusion coefficient contributed more than 70% of the NMR signal, which might be related to the Cryo-TEM results that suggest a volume fraction of 85% for the dilute domains. The absence of slower diffusive modes corresponding to mobility within the dense regions could be explained by the short NMR transverse relaxation time (T_2<1 ms). At the high PE:protein charge ratio, PDADMAC is constrained so strongly within the dense domains/clusters and intracluster spaces that its translational motions and local fluctuations are too slow to be detected by PFG-NMR.

The presence of the two fast modes (5–30% contribution to the PFG-NMR signal) required consideration of the motions of PDADMAC during the lifetime of the dense domains. As dense domains break up, polymer chains are released, creating a reservoir of excess PDADMAC within the intracluster regions. The concentration gradients arising from the release of the excess PDADMAC ions at the domain boundaries lead to short-range flows. Therefore, factors relevant with the lifetime of the dense domains also affect the occurrence of these concentration-gradient driven flows. For the PDADMAC-BSA coacervate, higher pH, lower ionic strength and higher polyelectrolyte molecular weight correspond to conditions with longer lifetimes for dense domains, and smaller diffusion coefficients.

3.4.4. Rheology of coacervates

Rheological studies have been crucial in determining the connectivity of the domains within the heterogeneous structure of coacervates. Frequency sweep measurements of PE–micelle [88] and PE-protein coacervates [104,30] showed similarities within the larger frequency range but were different at the low and high frequency

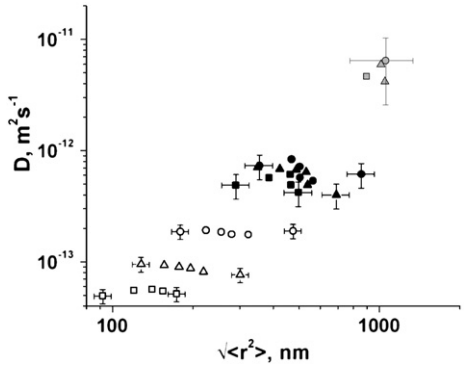

Fig. 17. Dependencies of the effective diffusivities of PDADMAC, within the PDADMAC-BSA coacervate, on the root mean square displacements calculated using the Einstein equation. Fractions fast1, fast2, and slow are indicated by gray, black, and empty symbols. Triangles show diffusivities for a coacervate prepared at pH = 7.7, *I* = 100 mM NaCl, polymer MW = 700 kDa; Circles for pH = 8.5, *I* = 100 mM, MW = 219 kDa; Squares for pH = 9.0, *I* = 50 mM, MW = 219 kDa [103].

ends: From 8 °C to 30 °C, PDADMAC/TX100-SDS micelles showed a dominant viscous character; i.e. G″>G′ between 0.1 and 1000 rad/s. However, polyelectrolyte-protein coacervates displayed a more complicated behavior. PDADMAC-BSA coacervates gave a solid-like response (G′>G″) — at low ω while Chitosan-BSA coacervates gave a solid like response at high ω. The inverse crossover frequency was 60–300 folds larger for Chitosan-BSA than for PDADMAC-BSA, indicating the longer lifetimes for interchain connectivities of the former.

3.4.4.1. Shear-thinning behavior. Shear thinning is a common behavior for coacervates of chitosan-BSA and PDADMAC-BSA [104,30] at 12 °C and 25 °C and for PDADMAC/TX100-SDS [88] at $T \geq T_{\varphi}'$. This last requirement is due to the coacervate structure at low T: a continuously interconnected network of dense domains with dilute regions as the "holes" (see Fig. 12); i.e. the continuous network at low T makes it harder to break the physical interactions by shear. At $T = T_{\varphi}'$, the viscosity of the coacervate shifts from Newtonian to shear-dependent. Formation of the shear-induced spherical 1 μm microdroplets has also been verified by SALS (Fig. 18), as mentioned above. Further increase of the shear rate results in a substantial drop of the viscosity, which is accompanied by transition of the spherical microdroplet to an ellipsoidal one with a diameter of 4 μm.

3.4.5. Small-angle neutron scattering (SANS) of coacervates

The length scales probed by FRAP, PFG-NMR, and DLS techniques, which yield the diffusion coefficients of macromolecules in coacervates, and rheology, which gives information about the connectivity of intercluster structures, are complementary to the length scales of SANS: ca. 80 μm for FRAP, hundreds nm to tens of μm for PFG-NMR, on the order of 250 nm for DLS, and a several nm's to a few hundreds of nm's for SANS. SANS scattering intensity curves were similar for Chitosan-BSA and PDADMAC-BSA coacervates at high scattering wave vector (q) values; i.e. both showing correlation peaks at length scales of $2\pi/q = 7.8 \pm 0.3$ nm. At length scales greater than 150 nm, chitosan-BSA coacervates displayed a ten-fold higher scattering intensity and a higher slope in the intensity vs. q curves than PDADMAC-BSA coacervates (Fig. 19). These data are explained by a coacervate model with more voluminous (more highly interconnected) dense domains for the Chitosan-BSA coacervates. The power-law dependencies at the intermediate q region, corresponding to 30–100 nm long structures, indicated string-like structures for Chitosan-BSA coacervates. At the same q-range, power law exponents were less than 1 for PDADMAC-BSA coacervates, pointing out to a disconnected/broken structure for the clusters/dense domains as shown in Fig. 11b. At the higher q-range, the scattering curves ended with a correlation peak, which was attributed to interprotein distance. The correlation length decreased with conditions of stronger electrostatic interaction (higher pH or lower I); i.e. 7.5–8.3 nm for PDADMAC-BSA coacervates and 7.8–8.1 nm for Chitosan-BSA coacervates vs. 8.9 nm for protein solutions with concentration comparable to those in coacervates (15–20%w:w). Thus, it is likely that proteins within the coacervate are less affected by interprotein repulsion compared to concentrated protein solutions. Dense domains of coacervates may sequester proteins at concentrations which would result in intense aggregation for polymer-free solutions.

4. Conclusions

Investigation of the mechanisms of complex formation between polyelectrolytes and oppositely charged colloids, and of coacervate structures formed at different length scales represents an active and important research area. While protein-polyelectrolyte systems are of particular importance. Polyelectrolyte-micelle systems represent a simpler model since micelles have isotropic geometry and charge density, in contrast to proteins with patchy surface charge and hydrophobicity. The complexation of polyelectrolytes and oppositely charged colloid is controlled by linear polymer charge density (ξ), surface colloid charge density and ionic strength (I). In addition to these key parameters, other system variables i.e. polymer molecular weight affect coacervation. Temperature and shear induced effects appear to be unique to micelle-polyelectrolyte systems. Models which focus on coacervation steps, such as the formation of complexes and their resultant aggregation and phase separation, consider the aggregates either as equilibrium complexes that reorganize within coexisting phases, or as soft colloidal particles whose interactions lead to clusters and phase separation. In the first type of models, equilibrium complexes may differ from each other in terms of disproportionation before phase separation. These may lead to complex internal structures within the polyelectrolyte/colloid coacervates, structurally heterogeneous on many length scales. Different coacervate morphologies have been demonstrated by techniques such as DLS, SANS, FRAP and PFG-NMR. Although mechanisms of coacervation have been deduced from observations of self-organized microscopic structures, the true relationship between coacervation mechanism and the resultant structure remains to be further explored.

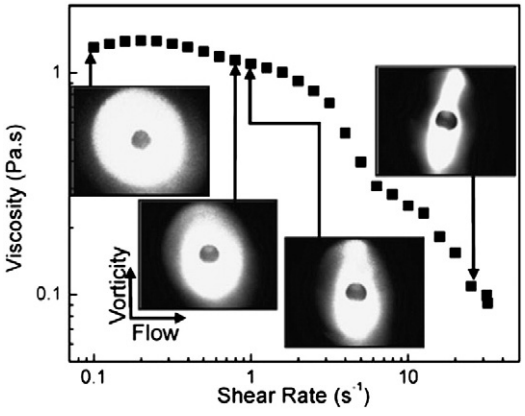

Fig. 18. Viscosity as a function of shear rate at 26 °C for a PDADMAC/TX100-SDS coacervate with inset SALS patterns [88].

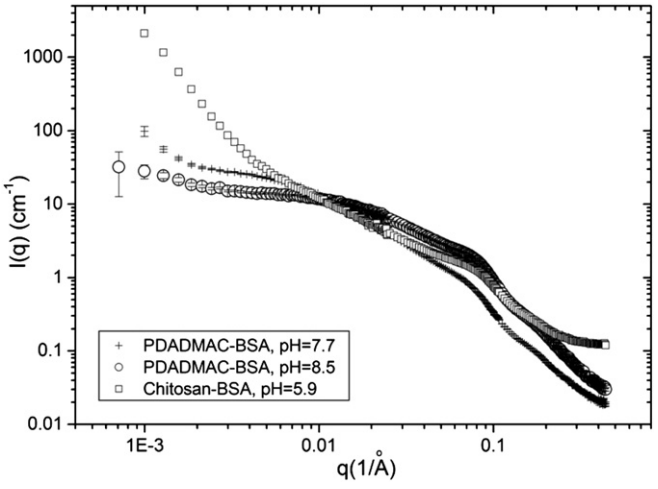

Fig. 19. Scattering intensity profiles for the chitosan-BSA and PDADMAC-BSA coacervates prepared at $I = 100$ mM with Mn = 140 kDa at pH 8.5 and 460 kDa at pH 7.7 [30].

References

[1] de Jong HGB, Kruyt HR. P K Akad Wet-Amsterd 1929;32:849.
[2] Cooper CL, Dubin PL, Kayitmazer AB, Turksen S. Curr Opin Colloid In 2005;10:52.
[3] Oparin AI. Vestn an Sssr+ 1980:57.
[4] Michaeli I, Overbeek JTG, Voorn MJJ. J Polym Sci 1957;23:443.
[5] Veis A, Bodor E, Mussell S. Biopolymers 1967;5:37.
[6] Sato H, Nakajima A. Colloid Polym Sci 1974;252:294.
[7] Tainaka KI. J Phys Soc Jpn 1979;46:1899.
[8] Wang YL, Kimura K, Huang QR, Dubin PL, Jaeger W. Macromolecules 1999;32:7128.
[9] Wang YL, Kimura K, Dubin PL, Jaeger W. Macromolecules 2000;33:3324.
[10] Singh SS, Siddhanta AK, Meena R, Prasad K, Bandyopadhyay S, Bohidar HB. Int J Biol Macromol 2007;41:185.
[11] Leisner D, Imae T. J Phys Chem B 2003;107:8078.
[12] Dubin PL, Gruber JH, Xia JL, Zhang HW. J Colloid Interface Sci 1992;148:35.
[13] SwansonVethamuthu M, Dubin PL, Almgren M, Li YJ. J Colloid Interface Sci 1997;186:414.
[14] Feng XH, Dubin PL, Zhang HW, Kirton GF, Bahadur P, Parotte J. Macromolecules 2001;34:6373.
[15] Dubin PL, The SS, Gan LM, Chew CH. Macromolecules 1990;23:2500.
[16] Wang YL, Dubin PL, Zhang HW. Langmuir 2001;17:1670.
[17] Gruber JV. J Cosmet Sci 2009;60:385.
[18] Jiang Y, Huang QR. Abstr Pap Am Chem S 2004;228:U396.
[19] Burgess DJ, Ponsart S. J Microencapsul 1998;15:569.
[20] Magnin D, Dumitriu S, Chornet E. J Bioact Compat Polym 2003;18:355.
[21] Wang YF, Gao JY, Dubin PL. Biotechnol Progr 1996;12:356.
[22] Jones OG, Lesmes U, Dubin P, McClements DJ. Food Hydrocolloid 2010;24:374.
[23] Stewart RJ, Weaver JC, Morse DE, Waite JH. J Exp Biol 2004;207:4727.
[24] Kaibara K, Okazaki T, Bohidar HB, Dubin PL. Biomacromolecules 2000;1:100.
[25] Xia JL, Zhang HW, Rigsbee DR, Dubin PL, Shaikh T. Macromolecules 1993;26:2759.
[26] Veis A. J Phys Chem-Us 1963;67:1960.
[27] Srivastava A, Waite JH, Stucky GD, Mikhailovsky A. Macromolecules 2009;42:2168.
[28] Kizilay E, Maccarrone S, Foun E, Dinsmore AD, Dubin PL. J Phys Chem B 2011;115:7256.
[29] Chollakup R, Smitthipong W, Eisenbach CD, Tirrell M. Macromolecules 2010;43:2518.
[30] Kayitmazer AB, Strand SP, Tribet C, Jaeger W, Dubin PL. Biomacromolecules 2007;8:3568.
[31] Michaels AS, Miekka RG. J Phys Chem-Us 1961;65:1765.
[32] A. Veis, The thermodynamics of complex coacervation phase separation. Advances in Colloid and Interface Science accepted.
[33] Vongoeler F, Muthukumar M. J Chem Phys 1994;100:7796.
[34] Muthukumar M. J Chem Phys 1987;86:7230.
[35] Girard M, Turgeon SL, Gauthier SF. J Agric Food Chem 2003;51:4450.
[36] Feng X, Leduc M, Pelton R. Colloids Surf A 2008;317:535.
[37] Ball V, Maechling C. Int J Mol Sci 2009;10:3283.
[38] Xia JL, Mattison K, Romano V, Dubin PL, Muhoberac BB. Biopolymers 1997;41:359.
[39] Mishael YG, Dubin PL. Langmuir 2005;21:9803.
[40] Wiegel FW. J Phys A: Math Gen 1977;10:299.
[41] Evers OA, Fleer GJ, Scheutjens JMHM, Lyklema J. J Colloid Interface Sci 1986;111:446.
[42] Kong CY, Muthukumar M. J Chem Phys 1998;109:1522.
[43] Park JM, Muhoberac BB, Dubin PL, Xia JL. Macromolecules 1992;25:290.
[44] Harnsilawat T, Pongsawatmanit R, McClements DJ. Food Hydrocolloid 2006;20:577.
[45] Seyrek E, Dubin PL, Tribet C, Gamble EA. Biomacromolecules 2003;4:273.
[46] Kayitmazer AB, Quinn B, Kimura K, Ryan GL, Tate AJ, Pink DA, et al. Biomacromolecules 2010;11:3325.
[47] Mcquigg DW, Kaplan JI, Dubin PL. J Phys Chem-Us 1992;96:1973.
[48] Wallin T, Linse P. Langmuir 1996;12:305.
[49] Kayitmazer AB, Seyrek E, Dubin PL, Staggemeier BA. J Phys Chem B 2003;107:8158.
[50] Weinbreck F, de Vries R, Schrooyen P, de Kruif CG. Biomacromolecules 2003;4:293.
[51] Odijk T. Langmuir 1991;7:1991.
[52] Zhang HW, Ohbu K, Dubin PL. Langmuir 2000;16:9082.
[53] Kayitmazer AB, Shaw D, Dubin PL. Macromolecules 2005;38:5198.
[54] Sperber BLHM, Schols HA, Stuart MAC, Norde W, Voragen AGJ. Food Hydrocolloid 2009;23:765.
[55] Winning H, Viereck N, Norgaard L, Larsen J, Engelsen SB. Food Hydrocolloid 2007;21:256.
[56] Cooper CL, Goulding A, Kayitmazer AB, Ulrich S, Stoll S, Turksen S, et al. Biomacromolecules 2006;7:1025.
[57] Mattison KW, Brittain IJ, Dubin PL. Biotechnol Progr 1995;11:632.
[58] Aberkane L, Jasniewski J, Gaiani C, Scher J, Sanchez C. Langmuir 2010;26:12523.
[59] Nigen M, Croguennec T, Renard D, Bouhallab S. Biochemistry 2007;46:1248.
[60] Rigsbee DR, Dubin PL. Langmuir 1996;12:1928.
[61] Gummel J, Cousin F, Boue F. J Am Chem Soc 2007;129:5806.
[62] Skepo M, Linse P. Phys Rev E 2002;66.
[63] Mcghee JD, Hippel PHV. J Mol Biol 1974;86:469.
[64] Malay O, Bayraktar O, Batigun A. Int J Biol Macromol 2007;40:387.
[65] Schmitt C, Sanchez C, Lamprecht A, Renard D, Lehr CM, de Kruif CG, et al. Colloid Surf B 2001;20:267.
[66] Chodankar S, Aswal VK, Kohlbrecher J, Vavrin R, Wagh AG. Phys Rev E 2008;78.
[67] Berret JF, Herve P. J Phys Chem B 2003;107:8111.
[68] Martinez-Tome MJ, Esquembre R, Mallavia R, Mateo CR. Biomacromolecules 2010;11:1494.
[69] Mekhloufi G, Sanchez C, Renard D, Guillemin S, Hardy J. Langmuir 2005;21:386.
[70] Li YJ, Xia JL, Dubin PL. Macromolecules 1994;27:7049.
[71] Li YJ, Dubin PL, Spindler R, Tomalia DA. Macromolecules 1995;28:8426.
[72] Michael Fisher private communication 1998.
[73] Antonov M, Mazzawi M, Dubin PL. Biomacromolecules 2010;11:51.
[74] Li YJ, Dubin PL, Havel HA, Edwards SL, Dautzenberg H. Langmuir 1995;11:2486.
[75] Kayitmazer AB, Bohidar HB, Mattison KW, Bose A, Sarkar J, Hashidzume A, et al. Soft Matter 2007;3:1064.
[76] Weinbreck F, Wientjes RHW. J Rheol 2004;48:1215.
[77] Zhang R, Shklovskii BT. Physica A 2005;352:216.
[78] Xu Y, Mazzawi M, Chen K, Sun L, Dubin P. Biomacromolecules 2011;12:1512.
[79] Doi R, Kokufuta E. Langmuir 2010;26:13579.
[80] Michaels AS. Ind Eng Chem 1965;57:32.
[81] Girard M, Turgeon SL, Gauthier SF. Food Hydrocolloids 2002;16:585.
[82] Cousin F, Gummel J, Clemens D, Grillo I, Boue F. Langmuir 2010;26:7078.
[83] Espinosa-Andrews H, Baez-Gonzalez JG, Cruz-Sosa F, Vernon-Carter EJ. Biomacromolecules 2007;8:1313.
[84] Lee AC, Hong YH. Food Res Int 2009;42:733.
[85] Kumar A, Dubin PL, Hernon MJ, Li YJ, Jaeger W. J Phys Chem B 2007;111:8468.
[86] Zhang B, Kirton GF, Dubin PL. Langmuir 2002;18:4605.
[87] Dubin PL, Li YJ, Jaeger W. Langmuir 2008;24:4544.
[88] Liberatore MW, Wyatt NB, Henry M, Dubin PL, Foun E. Langmuir 2009;25:13376.
[89] Lee LT, Cabane B. Macromolecules 1997;30:6559.
[90] Sanchez C, Despond S, Schmitt C, Hardy J. Food colloids: fundamentals of formulation. In: Dickinson E, Miller R, editors. Royal Society of Chemistry; 2001. p. 332.
[91] Veis A, Aranyi C. J Phys Chem 1960;64:1203.
[92] Meyer M, Le Ru EC, Etchegoin PG. J Phys Chem B 2006;110:6040.
[93] Groenewold J, Kegel WK. J Phys Chem B 2001;105:11702.
[94] Stradner A, Sedgwick H, Cardinaux F, Poon WCK, Egelhaaf SU, Schurtenberger P. Nature 2004;432:492.
[95] Archer AJ, Wilding NB. Phys Rev E 2007;76.
[96] Gummel J, Boue F, Deme B, Cousin F. J Phys Chem B 2006;110:24837.
[97] Gummel J, Cousin F, Verbavatz JM, Boue F. J Phys Chem B 2007;111:8540.
[98] Overbeek JT, Voorn MJ. J Cell Physiol Suppl 1957;49:7.
[99] Voorn MJ. Recl Trav Chim Pays-Bas Belg 1956;75:317.
[100] Gummel J, Boue F, Clemens D, Cousin F. Soft Matter 2008;4:1653.
[101] Wang Y. Protein separation via association with confined polyelectrolytes: coacervation and chromatography. West Lafayette, IN: Purdue University; 1998.
[102a] Burgess DJ. Complex coacervation: microcapsule formation. In: Dubin PL, editor. Macromol Complexes Chem Biol. Berlin, Germany: Springer; 1994. p. 285.
[102b] Bungenberg de Jong HG. Colloid science. In: Kruyt HR, editor. London, U.K: 1209 Elsevier; 1949. p. 433.
[103] Menjoge AR, Kayitmazer AB, Dubin PL, Jaeger W, Vasenkov S. J Phys Chem B 2008;112:4961.
[104] Bohidar HB, Dubin PL, Majhi PR, Tribet C, Jaeger W. Biomacromolecules 2005;6:1573.